Nitrogen grain-boundary passivation of In-doped ZnO transparent conducting oxide

D. Ali,[1,2] M. Z. Butt,[3] C. Coughlan,[2] D. Caffrey,[2,4] I. V. Shvets,[2,4] and K. Fleischer[2]
[1]*Department of Physics, GC University Lahore-54000, Pakistan*
[2]*School of Physics, Trinity College Dublin, The University of Dublin, College Green, Dublin 2, Ireland*
[3]*Centre for Advanced Studies in Physics, GC University Lahore-54000, Pakistan*
[4]*Centre for Research on Adaptive Nanostructures and Nanodevices (CRANN), Trinity College Dublin, The University of Dublin, College Green, Dublin 2, Ireland*

(Received 28 December 2017; published 9 April 2018)

We have investigated the properties and conduction limitations of spray pyrolysis grown, low-cost transparent conducting oxide ZnO thin films doped with indium. We analyze the optical, electrical, and crystallographic properties as functions of In content with a specific focus on postgrowth heat treatment of these thin films at 320 °C in an inert, nitrogen atmosphere, which improves the films electrical properties considerably. The effect was found to be dominated by nitrogen-induced grain-boundary passivation, identified by a combined study using *in situ* resistance measurement upon annealing, x-ray photoelectron spectroscopy, photoluminescence, and x-ray diffraction studies. We also highlight the chemical mechanism of morphologic and crystallographic changes found in films with high indium content. By optimizing growth conditions according to these findings, ZnO:In with a resistivity as low as 2×10^{-3} Ω cm, high optical quality ($T \approx 90\%$), and sheet resistance of 32Ω/□ has been obtained *without* any need for postgrowth treatments.

DOI: 10.1103/PhysRevMaterials.2.043402

I. INTRODUCTION

Transparent conducting oxides (TCOs) are a unique class of material that simultaneously possess both high optical transparency 85%–90% in the visible region and low electrical resistivity $\sim 10^{-4}$ Ω cm. TCOs are widely used in solar cells, light-emitting diodes, liquid-crystal displays, touch screen panels, and in some specific cases in gas sensors [1–7]. From a commercial standpoint the most widely utilized TCO is tin-doped indium oxide (ITO). The ubiquity of ITO can be attributed to its superior optical and electrical properties. However, high indium material costs, the need for sputter deposition, and its brittleness puts limits on its use in low-cost or flexible devices. As a result an alternative is highly desirable. To overcome these limitations, various alternative inexpensive as well as abundantly available materials have gained considerable attention. Among these various materials zinc oxide (ZnO) has emerged as one of the most promising candidates [8,9]. Intrinsic ZnO has a high optical transparency in the visible region, but a low electrical conductivity resulting from a low intrinsic carrier concentration. An effective way to improve ZnO electrical properties, without deteriorating the optical properties, is by doping with group-III elements (In, Al, and Ga). These materials substitute on the Zn site generating a shallow donor level, thereby increasing the carrier concentration [10,11]. In this work, we focus on indium doping, which has been found to be an effective means to improve electrical properties of ZnO [4,12–19].

Historically, the highest performance ZnO thin films have been prepared by physical vapor deposition (PVD) techniques such as sputtering [10,15,18] and pulsed laser deposition [20,21]. However, these processes are complicated by their dependence on high vacuum systems. On the other hand, thin films prepared by chemical vapor, or solution based methods (chemical bath deposition, sol-gel spin coating, and spray pyrolysis) are mechanically simple, can be performed at atmospheric pressure, facilitate large area coverage and simple composition control and therefore facilitate low production costs [19,22–27]. One of the major concerns with such low-cost methods is that the electrical conductivity of the produced ZnO typically suffers in comparison to best performing PVD prepared films. The lower performance of chemical vapor deposition (CVD) produced films typically originates from a combination of crystalline quality, a high number of grain boundaries, and the formation of a hydroxide/double hydroxide layer on the top and grain surface. To improve the electrical conductivity of ZnO films can be irradiated with ultraviolet (UV) light [28–30] or postannealed in reducing environments [28,31–33].

Several physical effects can contribute to conductivity changes in postgrowth treated ZnO including recrystallization, dephasing, generation, and reordering of extrinsic and intrinsic point defects and passivation of charge traps at grain boundaries. This creates a complex interplay of effects which are currently not well understood at a fundamental level, even if certain behaviors can be anticipated. The main objective of the present work is to decouple these effects by specifically investigating the passivation of grain boundaries using low-temperature nitrogen annealing. By containing this study to films annealed at temperatures substantially below the initial growth temperature, we exclude crystallographic changes upon annealing, allowing us to solely focus on the effects of the nitrogen passivation. The effect of the nitrogen annealing on the grain boundaries is discussed for a wide range of doping levels from 0.2% to 10%. Using the optimum dopant levels and N_2 postannealing, we demonstrate that ZnO:In with a resistivity as low as 5×10^{-3} Ω cm and a Hall mobility up to 7 $cm^2\,V^{-1}\,s^{-1}$

 ©2018 American Physical Society

is achievable using low-cost spray pyrolysis. The initial film properties are in line with previous reports on ZnO:In thin films grown by spray pyrolysis, metal-organic chemical-vapor deposition, or sputtering [19,34–36]. Here, we demonstrate how an understanding of the effect of annealing in a N_2 atmosphere was applied to modify growth conditions, achieving even better films with mobilities of up to 12 $cm^2 V^{-1} s^{-1}$ and resistivity of only 2×10^{-3} Ω cm without the requirements of *any postdeposition* treatment.

II. EXPERIMENTAL DETAILS

Undoped and In-doped ZnO thin films were deposited on glass substrates by spray pyrolysis at atmospheric pressure using a low-cost air blast nozzle. The distance between substrate and nozzle (PNR, MAD 0331) was 26 cm. 0.2 M molar solutions of zinc acetate dihydrate [$Zn(CH_3COO)_2 \cdot 2H_2O$] and indium chloride ($InCl_3$) in methanol were used as precursor solutions. Precursor solutions were mixed prior to deposition with In/Zn ratios of 0.2, 0.4, 0.6, 0.8, 1, 1.25, 1.5, 2, 2.5, 3.5, 5, and 10% nominal In concentration with respect to Zn. The liquid flow rate was set at 3 ml/min and nitrogen was used as a carrier gas with a flow rate of 15 l/min. Thin films were grown on heated glass substrates (420 °C) for 10 min following previously optimized conditions for ZnO:Al [27].

Thermal postgrowth treatments were carried out in full nitrogen atmosphere in a separate Bell-jar chamber. The thin-film resistivity was measured *in situ* by four-point probe measurements using spring loaded gold contacts in linear configuration with a Keithley 2400 source meter. The film resistivity was recorded during a 50 °C → 320 °C → 50 °C annealing cycle with a full process time of 15 min. Selected films were kept at 320 °C for a longer period until the conductivity improvement saturated. With the film thicknesses of 400 ± 50 nm used here, this was usually achieved after 5–10 min at 320 °C. Further electrical measurements of sheet resistance R_s, resistivity ρ, carrier mobility μ, and carrier concentration n_e were performed at room temperature before and after the N_2 annealing using a second Hall system in van der Pauw configuration using magnetic fields of up to 800 mT.

Room-temperature photoluminescence spectra were obtained from Edinburgh Instruments FL920 using a monochromized xenon lamp set to 325 nm excitation wavelength. Crystallographic information for all thin films was derived from the x-ray diffraction (XRD) patterns obtained using a Bruker D8 Advance with monochromized Cu $K\alpha 1$ radiation. Measured patterns have been analyzed and refined using the software package MAUD [37]. The surface morphology and grain structure of selected thin films was further studied by scanning electron microscopy (SEM) in a Zeiss Ultra Plus. Total and scattered transmittance (T_t,T_s) and total reflectance (R_t) spectra of all thin films were measured with a Perkin Elmer S650 spectrophotometer using an integrating sphere. These measurements were used to calculate the haze of the thin films ($H = T_s/T_t$). Interference fringes were used to calculate each film's thickness for the calculation of the resistivity from the measured sheet resistance R_s. All spectrophotometric measurements include the substrate contribution, using air as reference only.

Selected nitrogen-annealed indium-doped films were also analyzed by x-ray photoelectron spectroscopy (XPS) using a monochromized Al $K\alpha$ radiation in an Omicron MultiProbe XPS system. Spectra were taken before and after Ar ion etching (1.5×10^{-5} mbar, 750 eV ion energy, 12 μA ion current, for 5 min), to distinguish between bulk and surface stoichiometry of the ZnO films.

III. RESULTS AND DISCUSSION

A. Nitrogen annealing

For the In concentrations discussed here the as-deposited spray pyrolysis grown doped ZnO is already conductive without posttreatment. However, a dramatic improvement was noted if films are annealed in an inert, nitrogen atmosphere [27]. In order to determine the most dominant physical process for this notable enhancement, we investigated this process in more detail, using indium-doped ZnO (ZnO:In) rather than aluminum-doped ZnO (ZnO:Al) to (a) illustrate the universality of the process for group-III doped, spray pyrolysis grown ZnO and (b) as initial results showed an even higher achievable conductivity in ZnO:In compared to ZnO:Al grown in the same way. Figure 1 shows the electrical resistivity data of nominally undoped and In-doped ZnO thin films during their thermal treatment in nitrogen atmosphere at 50 °C → 320 °C → 50 °C. Qualitatively, the structure of the change in resistivity is the same for undoped and In-doped ZnO thin films and follows a set of successive regimes: During temperature ramp up the resistivity decreases as expected for a thermally activated nondegenerate semiconducting oxide (regime I), above approximately 200 °C the rate of change of the resistivity increases significantly (regime II), while on ramp down (regime III) it can be seen that the change in resistivity is permanent and only increases slightly, consistent with a semiconducting behavior of the ZnO. The magnitude of the decrease in electrical resistivity during this process, however, depends on the doping concentration, with highly doped films improving by about a factor of 3, while in nominally undoped films the change can be as high as a factor of 1000.

The temperature dependence of the resistivity of a homogeneous semiconducting film would typically follow an exponential law governed by the carrier activation energy E_a:

$$\rho = \rho_0 \exp\left[-E_a/(k_b T)\right]. \quad (1)$$

The changes in resistivity with temperature observed here are more complex as not only carriers are thermally activated, but also the material is altered in a permanent way. As a whole therefore, the observed nonmonotonic, hysteresis type change as a function of temperature cannot be expressed in a simple matter. Despite this, individual regions that follow simpler behaviors can be analyzed. For example, after the N_2 anneal, during cool down (regime III) Eq. (1) is valid as the change is predominantly driven by the carrier activation and the carrier activation energies can be determined by Arrhenius-type plots of data from regime III, found to be as low as $E_a \sim 6$ meV as expected for an almost degenerated TCO. In regime II (large change in ρ above 200 °C) the characteristic energy determined from the Arrhenius equation is much higher and varies from 0.8 eV for undoped to 0.2 eV for highly doped ZnO:In films. The magnitude of this characteristic energy already suggests

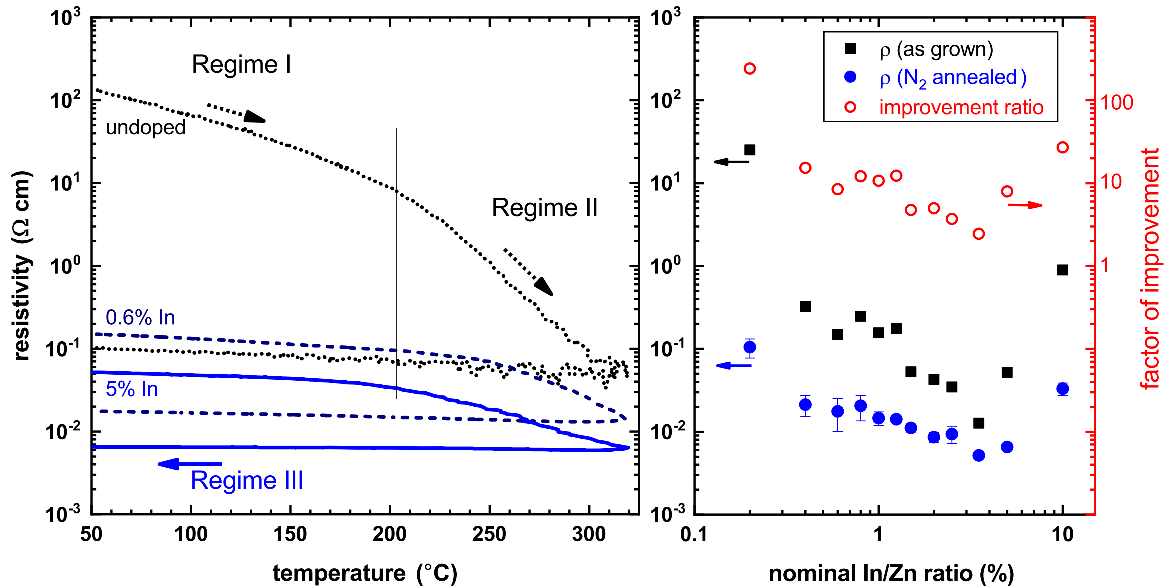

FIG. 1. Example of the measured resistivity of undoped ZnO and ZnO:In thin films (0.6% and 5%) as a function of temperature during the nitrogen anneal cycle. The observed hysteresis illustrates the significant reduction in resistivity. The right panel shows the resistivity before and after the anneal cycle for all films and the ratio of improvement.

that the root cause is an exchange of loosely bound species at the grain boundaries or bulk of the ZnO:In, as it is too high to be of electronic nature, but too low to indicate changes in the crystallographic nature which would require breaking of cation-oxygen bonds. Indeed, as the anneal temperature is significantly lower than the growth temperature, changes in the phase or crystal quality are not expected.

We therefore suggest the improvement in electrical response is caused by the removal of dangling bonds and chemisorbed species like OH, O_2^-, O^-, O^{--} at the grain boundaries in the presence of nitrogen at elevated temperature. Trap states at ZnO grain boundaries can increase the potential barrier for electron transport between grains, inhibiting the electron transport through the films [29,38–41]. A drawback of ZnO solution based growth is that hydroxide/double hydroxide layers can be formed on the surface of thin films, which has been reported to deteriorate the electrical properties [42,43]. The ZnO:In films grown here were prepared at 420 °C. While nitrogen was used as carrier gas, oxygen species (O_2^-, O^-, and O^{--}) are available from the hydrogenated salts used as precursor, the surrounding atmosphere prior growth, and in the form of CO and CO_2, as combustion reactants of the methanol solvent. All of these can get chemisorbed at the grain boundaries, specifically during the postgrowth cool down, where films are exposed to the atmosphere within the spray pyrolysis chamber. The chemisorption and desorption of such oxygen species has been previously studied as a function of temperature as well as on the metal oxide [44–46]. For temperatures below 100 °C, O_2^- gets chemisorbed on the surface, at temperatures between 100 °C and 300 °C O^- species becomes dominant, and for temperatures higher than 300 °C the probability for chemisorption of O^{--} becomes very high. Within our model, during annealing in nitrogen above 200 °C the oxygen species induced trap states within the grain boundaries are removed, either by removal of the oxygen molecular species or their replacement with neutral nitrogen molecules. As a consequence we would expect the reduction in film resistivity to be dominated by gains in electron mobility. Other explanations such as an activation of the dopant by removal of compensating defects would, in contrast, increase the carrier concentration.

Figure 2 compares the resistivity, carrier mobility, and carrier concentration of ZnO:In thin film determined by Hall measurements in van der Pauw geometry before and after the N_2-anneal cycle. For all films the Hall mobility is significantly improved after the N_2-anneal cycle. Within the experimental error, the carrier concentration was found to remain constant, or only decrease slightly. Only for undoped and low nominal doping concentrations below 0.3% was an increase in carrier concentration seen. The behavior is consistent with efficient extrinsic doping by the use of $InCl_3$ as precursor, which does not require postgrowth activation, only grain-boundary passivation. The electron mobility is not equally improved for all doping levels as the impact of the grain boundaries itself is a function of carrier concentration. With a given trap density n_T the trap induced depletion zone ($l_d \sim n_T/n_c$) within the grains is inversely proportional to their bulk carrier density n_c. Assuming a tunneling process for electrons, an increased depletion layer thickness will then exponentially increase the overall resistance. Hence, a reduction in n_T leads to a more significant decrease in the resistance of low-doped samples compared to highly doped ones. For nominally undoped samples, as-grown films were too resistant to be able to measure the Hall effect, while after N_2 treatment the resistivity was reduced by three orders of magnitude and already a Hall mobility $\mu_H = 0.3$ cm^2 V^{-1} s^{-1} was observed. For high doping levels μ_H was found to be as high as 7 cm^2 V^{-1} s^{-1}, although this was found to decrease again above nominal In concentrations of 3.5% as other effects such as ionized impurity scattering and morphological changes within the films become more important. It is noteworthy that ZnO:In has previously been

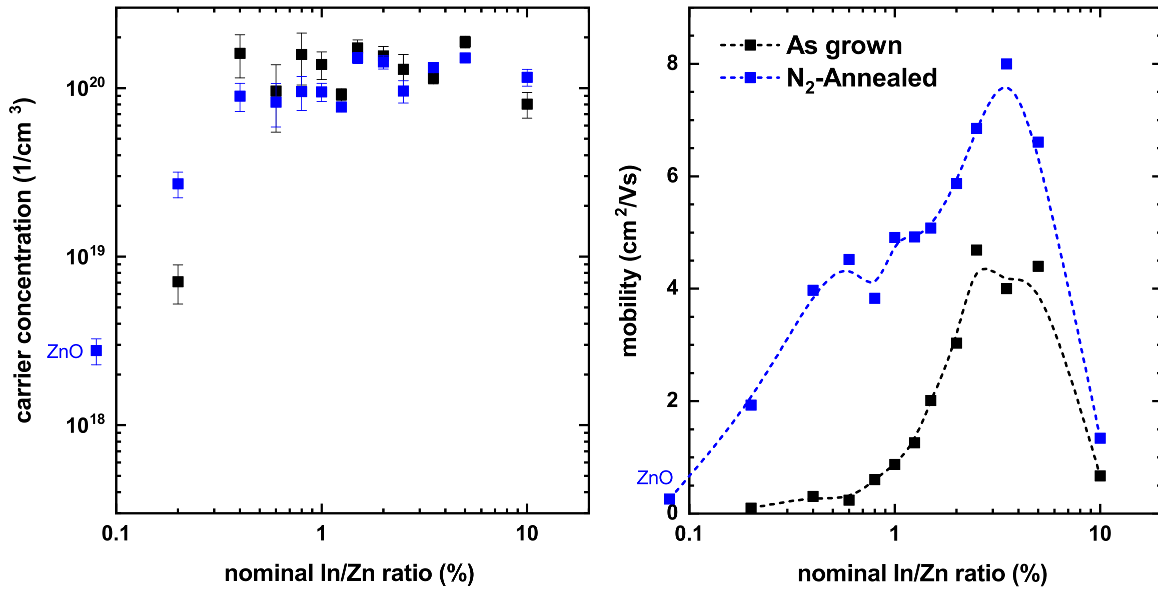

FIG. 2. Carrier concentration and Hall mobility of as-grown (black) and N_2 annealed (blue) ZnO:In. The decrease in resistivity during the anneal cycle is predominantly caused by a change in carrier mobility. Only for nominally undoped samples and In content below 0.4% was an increase in carrier concentration during annealing noted.

used in H_2S sensing, where the proposed mechanism of the resistance decrease upon H_2S exposure was likewise a reaction with oxygen species at the grain surface [7].

So far we have shown indirect evidence that the nitrogen passivates the ZnO grain boundaries. We now directly demonstrate this change using XPS of a ZnO:In sample. Figure 3 shows the XPS data of a postannealed thin film. By XPS we can qualitatively show that there is a measurable nitrogen signal found in N_2-annealed samples, indicating an incorporation of N_2 molecules at the surface of grains. Once the top surface of the as-grown layers are removed in-vacuum by Ar ion etching the intensity of the N 1*s* core level is significantly reduced and the shape and intensity of the O 1*s* core level is substantially altered as surface hydroxide and carbonate compounds are removed. Likewise the nitrogen signal is reduced, as only a much smaller fraction of grain boundaries are still measured after ion etching, indicating that the N is heavily localized at the surface grain boundaries (see schematics in Fig. 3).

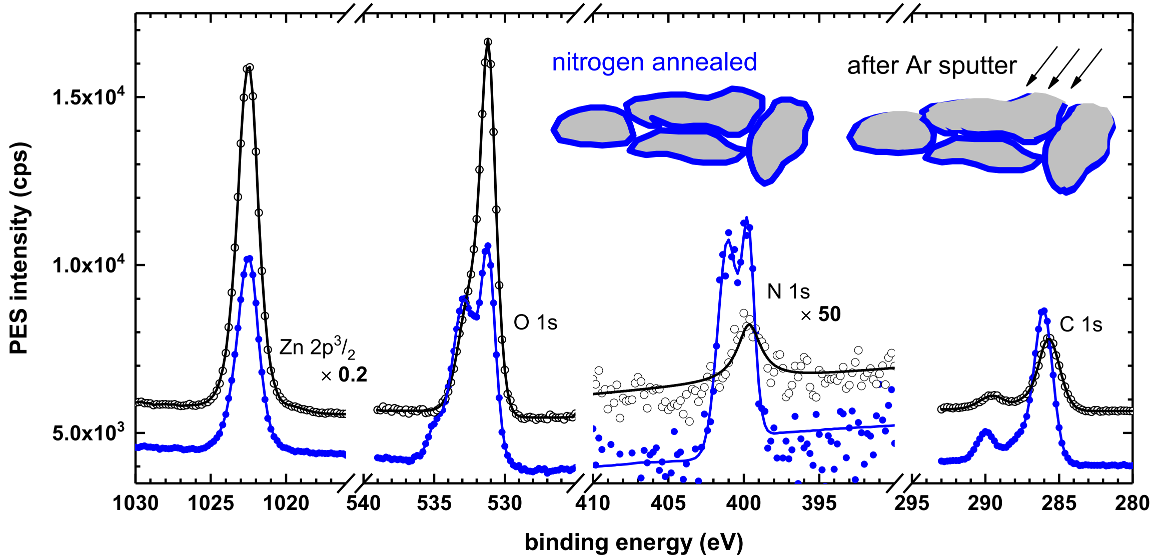

FIG. 3. XPS spectra of a ZnO:In sample after a nitrogen anneal cycle (blue) and *in situ* Ar ion etching (black), removing the samples top layer. The weak N 1*s* signal with two structures at 399.8 and 401.0 eV is significantly reduced after short Ar-ion etching removing approximately 1 nm of material. Additional oxygen components (OH, C−O, C=O) and residual carbon are also reduced, while the Zn 2*p* and O 1*s* (Zn-O) signal increases. Raw data (symbols) and fitted lines are shown. Zn signals have been scaled by a factor of 0.2, the weak nitrogen by a factor of 50, and in addition constant offsets have been employed for better visual comparison of the components and spectra.

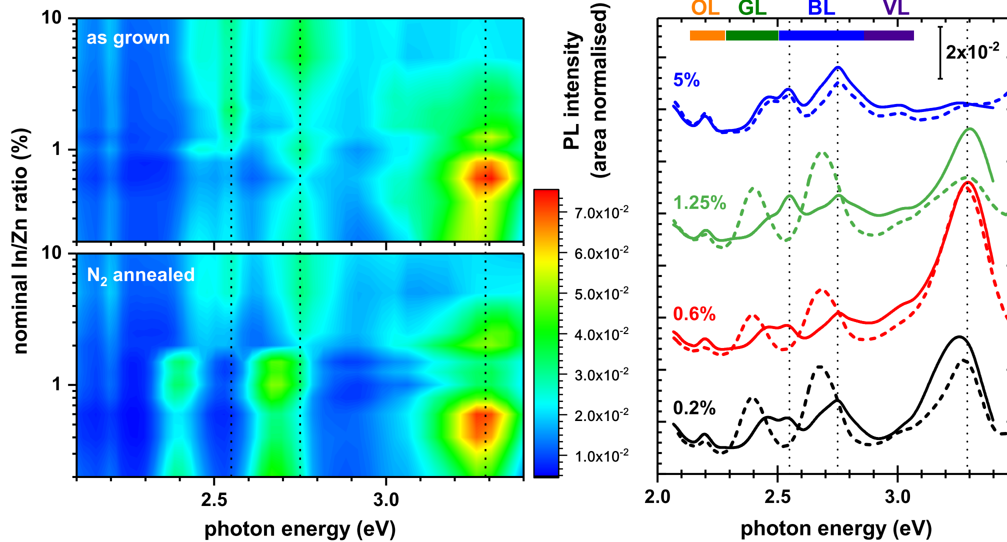

FIG. 4. Room-temperature photoluminescence measurement of ZnO:In films before and after nitrogen annealing. The spectra have been area normalized for easier comparison. Most prominently the green and blue defect luminescence intensity and energetic position is altered during the anneal process for doping levels below 2%. The spectra of 0.2, 0.6, 1.25, and 5% samples prior (solid lines) and after N_2 anneal (dashed lines) are shown exemplary on the right with characteristic features of as-grown films at 3.3, 2.74, and 2.54 eV indicated for better comparison. The spectral ranges for various defect emission bands (orange, green, blue, and violet) are indicated. False color plots are generated by extrapolating 12 discrete spectra with 0.2%–10% In content (see experimental details).

Further N_2 annealing of the Ar-ion etched surface under the same conditions as the first anneal cycle (a) did not further alter the conductivity as all grain boundaries where already passivated, but (b) also did not lead to a significant recovery of the N 1*s* core level signal. The latter illustrates that the N 1*s* signal for the first cycle measurement did not simply originate from loosely surface adsorbed molecular N_2 but involves a stronger interaction, presumably with the hydroxide layer as it was not observed for the Ar-ion etched hydroxide free surface. A two-component fit of the N 1*s* signal shows energetic positions of 399.8 and 401.0 eV, consistent with, e.g., C–N and C=N bonds [47]. However, we have to stress that at this point no clear identification of the chemical environment of the nitrogen can be given, as also strongly physisorbed N_2 molecules, e.g., on clean metallic surfaces, can show doublets in the N 1*s* signal [48]. Likewise we cannot directly assign the fine structure of the O 1*s* core level due to the inhomogeneity of our surfaces. In spray pyrolysis grown films we will have oxygen from the ZnO itself, but the surface sensitivity of XPS leads to additional signals from surface hydroxides as well as residual, unreacted or partially reacted precursors. As the organic solvent as well as the zinc precursor itself contains oxygen in different configurations we have a variety of possible species leading to the broad complex structure.

B. Photoluminescence

As XPS only probes the surface region it does not directly give information about the stoichiometry and point defects within the ZnO grains. We therefore investigated the photoluminescence of the ZnO films, previously demonstrated to provide insight on ZnO defect structure [49,50]. The room-temperature photoluminescence (PL) spectra of In-doped ZnO thin films before and after thermal treatment are shown in Fig. 4. As absolute PL intensities depend on focal conditions, film thickness, and film morphology, we only show area normalized spectra to discuss relative intensity changes of different luminescent centers. The spectra show the characteristic UV emission peak at 3.3 eV (376 nm) corresponds to near band edge emission due to electronic transition from near conduction band to valence band [51]. Defect induced PL emission is typically classified into 3–4 spectral regions (yellow/orange, green, blue, violet) with exact energetic positions, and relative intensities strongly depending on defect concentration and type, ZnO microstructure and morphology, and excitation wavelength [49,50,52]. The emission spectrum of as-grown ZnO:In exhibits prominent luminescence centers at the band edge (3.3 eV), and the blue/green region at 2.76 eV (BL), and 2.54/2.45 eV (GL). Weaker emissions are seen at 3.0 eV (VL) and 2.2 eV (OL). The peaks are seen for all dopant concentrations, but relative intensities vary. With an initial increase of In concentration up to 0.8% the relative intensity of the band edge luminescence increases, indicating an improved crystalline quality and is consistent with a consequent reduction in GL upon donor doping [52]. Above 1% In concentration it dramatically decreases again and the PL spectra are dominated by the blue/green defect luminescence.

Upon nitrogen annealing the behavior again depends on the dopant concentration. For highly doped films (>2%), dominated by the green and blue defect emission no significant changes in the relative PL intensities are observed. For lower dopant concentration the spectral position of the blue and green luminescence peaks is redshifted, their relative intensity increases, and only two distinct features at 2.67 eV (BL) and 2.39 eV (GL) remain. The band edge luminescence and weaker VL structure remain largely unchanged, while the weak OL structure is not changed in position but reduced in relative

intensity. The observed changes in the photoluminescence spectra can be qualitatively understood. The band edge and VL structures remain unchanged as the short nitrogen anneal does not alter the crystalline quality and number of zinc interstitials (Zn_i) associated with the VL emission [50,53]. In contrast the increased intensity of the BL and GL bands either indicates an increased number or luminescence efficiency of deep level defects such as single or double charged oxygen vacancies (V_O^+, V_O^{++}) [49,50]. It was noted that the presence of oxygen species at grain boundaries (O_2^-, O^-, and O^{--}) can quench the V_O related luminescence via nonradiative recombination processes [50]. The relative increase of the BL and GL emission after grain-boundary passivation is therefore expected and does not necessarily indicate a change in the number of defects. The observed energetic shift is likely a consequence of changes in the deep level defect charge state (e.g., V_O^{++} to V_O^+) induced by the removal of negatively charged surface oxygen species, or removal of interstitial hydrogen.

C. Structural and morphological properties

So far we have shown that the changes of the electrical properties of ZnO:In upon nitrogen annealing are caused by surface passivation, relatively independent of the actual doping concentration. The crystallographic properties of the ZnO:In, however, strongly changes with the dopant concentration. The x-ray diffraction patterns after thermal treatment in nitrogen atmosphere are shown in Fig. 5(a). The x-ray diffraction patterns clearly show that undoped thin films are of polycrystalline nature and exhibit hexagonal wurtzite structure (JCPDS No. 36-1451). A strong reflection corresponding to the (002) plane has been observed for low-doped ZnO thin films with dopant concentration in the range 0.2%–2%. It clearly shows that a preferred growth direction lies along the c axis. Raising the dopant concentration above 2% leads to a decline in (002) texture and almost completely randomized grain orientation. All peaks observed can be assigned to ZnO, suggesting there is no significant dephasing, and the aforementioned grain boundaries are thin enough, not to give rise to specific XRD patterns of hydroxides.

To obtain quantitative information regarding preferential orientation, the texture coefficient (TC) for the (002) and (101) planes was explicitly calculated using [54,55]

$$\mathrm{TC}(hkl) = \frac{I(hkl)}{I_0(hkl)}\left[\frac{1}{n}\sum_{i=1}^{n}\frac{I(h_ik_il_i)}{I_0(h_ik_il_i)}\right]^{-1}. \quad (2)$$

I and I_0 are the observed and standard diffraction intensity of the (hkl) plane, respectively, and n is the number of diffraction peaks in the XRD pattern. Here the six reflexes marked in Fig. 5(a) have been used for the texture analysis. Up to 1% In TC_{002} is above a value of 5. A subsequent increase of the In content quickly randomizes grain orientation, with films grown at 2.5% already showing a fully random grain orientation ($TC_{002} = 1$). Consequently the TC_{101} value of the (101) plane is much smaller (<0.2) for up to 1% In and raises to 1 for 2.5% In. Above 1% In content the average grain size also decreases.

According to Vegard's law, an inclusion of impurity atoms with larger ionic radius (In = 0.094 nm) on a substitutional site (InZn), replacing the small ionic radius (Zn = 0.074 nm) cation, will lead to a lattice expansion. Figure 5 shows the a- and c-axis lattice parameters of ZnO:In extracted from Rietveld refinement of the measured XRD patterns, compared to database ZnO. The spray pyrolysis grown material already has a slightly expanded lattice due to an increased number of intrinsic defects such as Zn_i, V_O, the presence of extrinsic

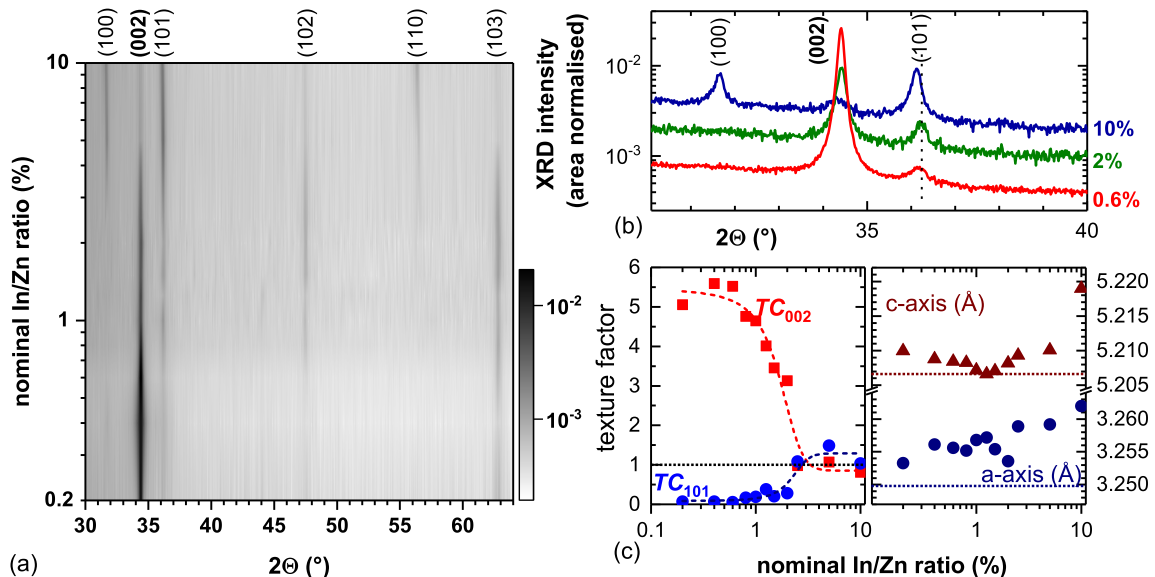

FIG. 5. (a) XRD patterns of ZnO:In as a function of the In/Zn ratio. Films up to 1% In/Zn ratio are highly textured with the ZnO c axis perpendicular to the surface. The gray-scale plot is generated by extrapolating 12 discrete diffraction patterns of samples with 0.2%–10% In content. (b) Close-up of the region around 2Θ values of 35° for low, medium, and highly doped films showing the change in texture and small shift to lower angles. (c) shows calculated texture coefficients for the (002) and (101) reflex and a- and c-lattice parameters derived from a Rietveld refinement of the XRD data. Dashed lines indicate the expected values for wurtzite ZnO (JCPDS pattern No. 36-1451).

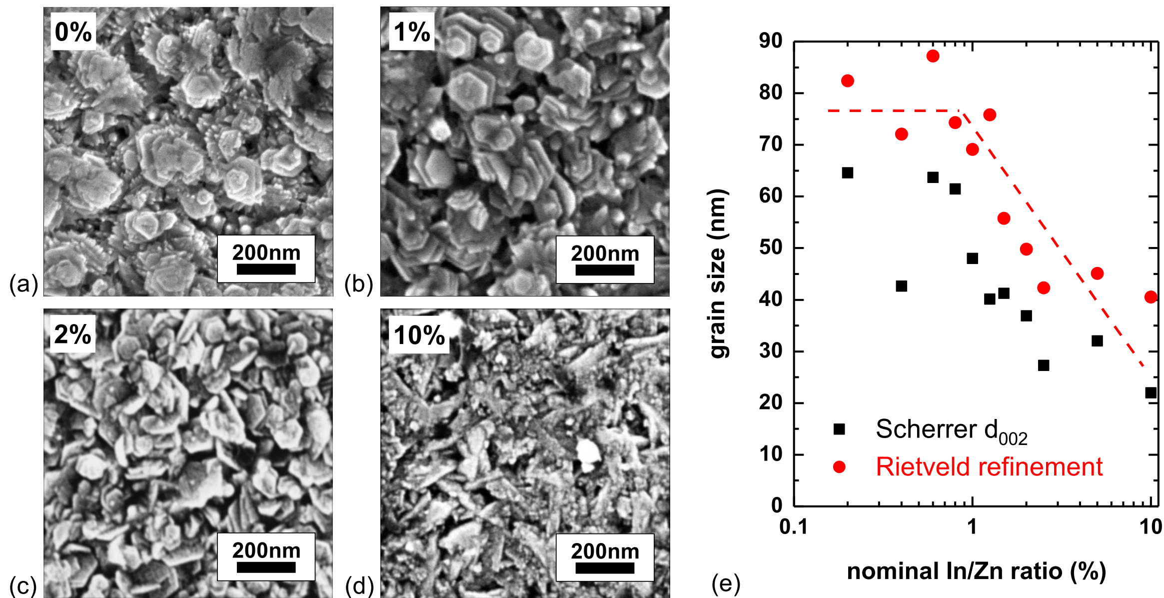

FIG. 6. (a)–(d) Scanning electron microscopy images of ZnO:In after N_2 annealing with increasing In/Zn ratio ($1 \times 1\ \mu$m area). The films are made of compact layers of stacked ZnO grains. Individual grains show a hexagonal structure. For low In/Zn ratio they are vertically stacked, while for higher concentration grains are randomly tilted. (e) There is also an overall reduction of grain size, consistent with the coherent domain size reduction as derived from Rietveld refinements of the measured XRD patterns and using the Scherrer equation for the (002) reflex.

residual dopants such as hydrogen interstitials, or residual carbon incorporation. Indium substitution does further expand the lattice; however, in contrast to high-temperature solid-state solutions of ZnO:In [56] no solubility limit is seen, even up to 10% atomic In/Zn ratio. Furthermore the *c*-axis lattice parameter changes nonmonotonically with In content and a small In concentration up to 1% even reduces the observed deviations from the bulk values. This can be understood if either the introduction of the In_{Zn} substitutional sites or the presence of a small amount of Cl^- ions in the solution suppresses the formation of other intrinsic or extrinsic defects. This finding explains the improved overall quality of the films (higher texture, larger grain size, less defect luminescence) for films with In content in the 0.6%–1% range. Further increases of the In content, however, does lead to a lattice expansion in the *c* and *a* axes, accompanied with a deterioration of crystalline quality: the coherent domain size (e.g., grain size) reduces; ZnO grains within the films are found in various orientations. SEM images (see Fig. 6) illustrate these changes, as films visually look different with smaller, randomly oriented crystallites being clearly seen for highly doped films. All images where taken after nitrogen annealing. A qualitative comparison of images from earlier samples, which were not annealed, show no alterations of overall grain structure, as expected for a short annealing cycle, substantially below the growth temperature. For low doping levels, hexagonal-shaped grains grow on the basal plane in a direction perpendicular to the substrate. These individual grains form a columnar structure with decreasing grain size towards the film surface. The growth of hexagonal stacks perpendicular to the substrate clearly shows that the preferred orientation of the thin film lies along the *c* axis, which is well supported by XRD measurements. With the increase in dopant concentration the number of tilted hexagon stacks increases, size decreases, and the angle of tilt with respect to surface normal is more random. The core reason for these changes in crystal size and orientation is not necessarily the dopant-induced strain, as, e.g., isovalent Mg substitution in spray pyrolysis grown $Zn_{1-x}Mg_xO$ has seen much larger variations of the ZnO *a* and *c* axes, and Mg/Zn ratios of up to 35% without any detrimental effects on film texture or grain sizes [57]. The key difference is that *only* organic salts have been used for $Zn_{1-x}Mg_xO$ as the precursor for Zn and the substitutional Mg. In the case of indium substitution the equivalent indium acetate could not be used as it was found to be insoluble in methanol. Instead $InCl_3$ has been used. In conjunction with the H_2O molecules from the dihydrogenated zinc acetate precursor a small amount of HCl can be formed once the In content is increased. ZnO is easily etched in HCl, with complex etch patterns being observed dependent on the ZnO defect density and the amount of water added to the etching solution [58]. We therefore conclude that for In/Zn ratios well above 1%, the molarity of HCl formed in the precursor solution reaches a critical concentration, leading to substantial changes in the preferred nucleation direction (e.g., by selectively etching along the *c* axis) and overall grain size. It is therefore possible that the material quality of spray pyrolysis ZnO:In can be further improved by using chlorine-free, preferably organic precursors. A small amount of HCl etching could still be beneficial for the films, as initially the measured crystalline quality improves up to 1% In/Zn ratio. SEM images show smoother grains for the 1% sample, with the absence of small whiskers at the grain edge seen for undoped ZnO [see Figs. 6(a) and 6(b)]. We attribute this to a preferred etching of these small protrusions by small amounts of HCl formed. We have to stress that the exact nature of the ZnO texture and grain orientation in spray pyrolysis grown material crucially depends on the solvent employed. Hence the mechanism proposed here is limited to organic solvent

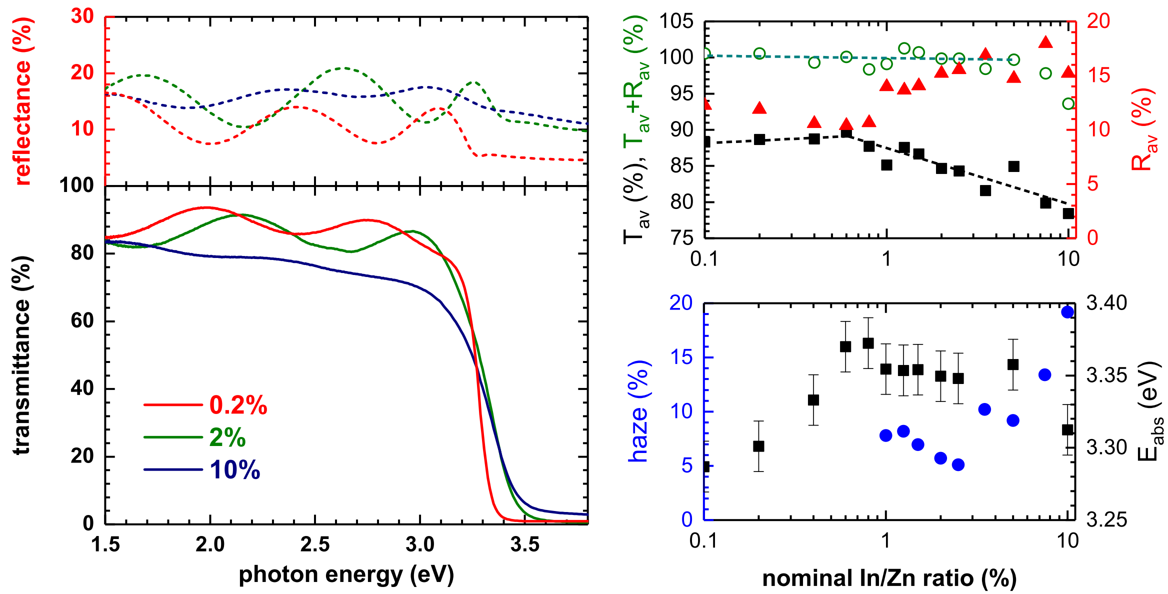

FIG. 7. Selected optical properties of the ZnO:In films. All films show a high transparency in the visible range with clearly defined thin-film interference fringes. The latter are used to calculate the film thickness d. The onset of optical absorption (E_{abs}), haze (H), and average sample transmittance and reflectance (T_{av}, R_{av}) is also shown.

solutions. Once water is mixed, or used as the sole solvent the details of the grain structure will differ dramatically [26,27,35].

D. Optical properties

Despite the noticeable deterioration of the ZnO:In crystalline quality the overall film quality remains high. Compact thin films are produced with high transparency in the visible region, well-defined thin-film interference fringes, and low haze. Figure 7 shows transmission and reflectance data for low-, medium-, and highly doped ZnO:In as well as parameters derived from these measurements for all films (average transmission T_{av}, onset of optical absorption E_{abs}, haze H, film thickness d). The small decrease in average optical transmittance in the visible region from 88% to 78% on increase in dopant concentration is, however, not caused by free carrier absorption, but rather is a consequence of the altered crystallographic texture. ZnO, as an anisotropic material, has a different refractive index for light polarized along or perpendicular to the c axis. By altering the thin films from preferentially c-axis-oriented films to randomly oriented grain, we consequently increase the thin films refractive index slightly. This is seen as an increase in the average reflectance measured on the same samples. Within the errors of the measurement, $T + R$ values are consistently at 100%, showing no significant absorption within the films in the 1.5–3.0 eV spectral range. There is a small increase in the onset of the optical absorption as determined by Tauc plots [extrapolating $(\alpha E)^{1/2}$ vs E plots]. This value is frequently interpreted as band gap E_g, but due to the strong excitonic nature of the onset of absorption and other systematic errors of this method for polycrystalline ZnO, such a Tauc analysis underestimates the band gap of ZnO [59]. We therefore refer to the quantity as the onset of absorption E_{abs}, important for a transparent conducting contact material.

The measured value of E_{abs} for undoped ZnO thin films is found to be 3.27 eV, in good agreement with the values reported in literature [18,21,23,24]. In line with the improvements in crystalline quality E_{abs} increases for dopant concentration up to 0.6%, reaches a plateau around ≈3.35 eV for In/Zn ratios between 0.6% and 5.0%, and decreases to 3.32 eV for 10% In/Zn ratio, once the In-induced lattice expansion dominates, and crystalline quality deteriorates again.

The blueshift in E_{abs} upon doping is also frequently attributed to the Burstein-Moss effect (BM) in degenerative doped materials once the increased carrier concentration lifts the Fermi level into the conduction bands [6,60]. The carrier concentration observed here is below that threshold, and resistance vs temperature measurements show semiconducting behavior. The changes in the optical gap are therefore dominated by crystallographic and grain size changes discussed above.

E. Optimized cool down procedure

We have illustrated that the main limitation to the ZnO:In conductivity of spray pyrolysis grown material is nonpassivated grain boundaries and brief nitrogen anneal cycles can remove charged oxygen species at these grain boundaries. Applying this knowledge we have subsequently modified our growth conditions to further improve the material:

(1) The growth chamber is purged with nitrogen, removing the ambient air out of the system prior to growth.

(2) Nitrogen purging is continued during the cool down of samples, maintaining an oxygen-poor atmosphere and effectively performing the postgrowth nitrogen anneal within the growth chamber itself.

(3) The sample is only removed once it has cooled down below 100 °C in order to prevent reoxidation of the grain boundaries.

(4) Growth rate is reduced by 25% using 0.15 M solutions, leading to an increase in overall grain size and hence reduction of the number of grain boundaries.

By adhering to all these procedural changes the postgrowth anneal cycle is no longer required and as-grown samples are as performant. Indeed using these optimized conditions the overall conductivity of as-grown films is already surpassing those of postgrowth annealed samples without the pregrowth and postgrowth nitrogen purge of the spray system. ZnO:In films, using 3.5% In/Zn ratio show degenerate doping, a resistivity as low as 2×10^{-3} Ω cm, and Hall mobility of 11.6 $cm^2/V\,s$ in 600-nm-thick films. Such values are approaching the performance of high-quality, sputtered or CVD epitaxially grown ZnO, despite using a low-cost, large-area chemical synthesis route.

IV. CONCLUSIONS

We have synthesized highly transparent ZnO thin films doped with 0.2%–10% In, on glass substrates at 420 °C by low-cost spray pyrolysis. The conductivity in as-grown films is limited by grain boundaries, specifically charged oxygen species formed during growth and cool down in the postgrowth atmosphere. Brief nitrogen annealing at 320 °C is sufficient to passivate the grain boundaries and significantly improve these films' electrical and luminescent properties. The best conductive films are found in the doping range of 1%–4%, with higher doping levels (>2%) deteriorating the crystalline quality of the films due to the use of a chlorine precursor. Using optimized growth conditions which minimize the exposure to atmospheric oxygen at all stages of the growth process, resistivities as low as 2×10^{-3} Ω cm and mobilities of 12 $cm^2/V\,s$ are achievable in spray pyrolysis grown ZnO:In. These films have 90% transmission with air as reference and a sheet resistance of 32 Ω/□, sufficient for cost-sensitive, large-area TCO applications, e.g., in smart windows, organic, thin-film, or silicon heterojunction solar cells.

ACKNOWLEDGMENTS

The authors acknowledge funding by Science Foundation Ireland under Grant No. 12/IA/1264. D.A. is grateful to the Higher Education Commission, Islamabad (1-8/HEC/HRD/2016/6307, PIN: IRSIP 33 PSc 04) for financial support under the International Research Support Initiative Program for Trinity College, University of Dublin.

[1] D. Ginley, H. Hosono, and D. C. Paine, *Handbook of Transparent Conductors* (Springer, New York, 2011).
[2] C. G. Granqvist, Sol. Energy Mater. Sol. Cells **91**, 1529 (2007).
[3] B. G. Lewis and D. C. Paine, MRS Bull. **25**, 22 (2000).
[4] S. Pati, P. Banerji, and S. B. Majumder, RSC Adv. **5**, 61230 (2015).
[5] K. Ellmer, Nat. Photonics **6**, 809 (2012).
[6] A. Klein, C. Korber, A. Wachau, F. Sauberlich, Y. Gassenbauer, S. P. Harvey, D. E. Proffit, and T. O. Mason, Materials **3**, 4892 (2010).
[7] S. S. Badadhe and I. Mulla, Sens. Actuators B **143**, 164 (2009).
[8] B. Cho, H. Kim, D. Yang, N. K. Shrestha, and M. M. Sung, RSC Adv. **6**, 69027 (2016).
[9] C. F. Klingshirn, B. K. Meyer, A. Waag, A. Hoffmann, and J. Geurts, *Zinc Oxide—From Fundamental Properties Towards Novel Applications*, Springer Series in Materials Science (Springer-Verlag, Berlin/Heidelberg, 2010), p. 300.
[10] M. Tadatsugu, S. Hirotoshi, N. Hidehito, and T. Shinzo, Jpn. J. Appl. Phys. **24**, L781 (1985).
[11] K. Ellmer and A. Bikowski, J. Phys. D **49**, 413002 (2016).
[12] K.-M. Chang, S.-H. Huang, C.-J. Wu, W.-L. Lin, W.-C. Chen, C.-W. Chi, J.-W. Lin, and C.-C. Chang, Thin Solid Films **519**, 5114 (2011).
[13] M. Faiz, A. Qurashi, and N. Tabet, Vacuum **130**, 159 (2016).
[14] S. Ghosh, M. Saha, and S. K. De, Nanoscale **6**, 7039 (2014).
[15] S. Hui, J. Shien-Uang, C. Sheng-Chi, Y. Shiau-Shiang, and W. Xin, J. Phys. D **50**, 045102 (2017).
[16] J.-W. Jeon, D.-W. Jeon, T. Sahoo, M. Kim, J.-H. Baek, J. L. Hoffman, N. S. Kim, and I.-H. Lee, J. Alloys Compd. **509**, 10062 (2011).
[17] S. Jongthammanurak, T. Cheawkul, and M. Witana, Thin Solid Films **571**, 114 (2014).
[18] A. Singh, S. Chaudhary, and D. K. Pandya, Acta Mater. **111**, 1 (2016).
[19] K. Tang, S. Gu, J. Liu, J. Ye, S. Zhu, and Y. Zheng, J. Alloys Compd. **653**, 643 (2015).
[20] V. L. Kuznetsov, A. T. Vai, M. Al-Mamouri, J. Stuart Abell, M. Pepper, and P. P. Edwards, Appl. Phys. Lett. **107**, 232103 (2015).
[21] V. Craciun, J. Elders, J. G. E. Gardeniers, and I. W. Boyd, Appl. Phys. Lett. **65**, 2963 (1994).
[22] K. J. Chen, F. Y. Hung, S. J. Chang, and Z. S. Hu, Appl. Surf. Sci. **255**, 6308 (2009).
[23] D. Ali, M. Z. Butt, B. Arif, A. A. Al-Ghamdi, and F. Yakuphanoglu, Phys. B (Amsterdam, Neth.) **506**, 83 (2017).
[24] D. Ali, M. Z. Butt, I. Muneer, F. Bashir, and M. Saleem, Optik **128**, 235 (2017).
[25] D. Ali, M. Z. Butt, B. Arif, A. G. Al-Sehemi, A. A. Al-Ghamdi, and F. Yakuphanoglu, Mater. Res. Express **4**, 026405 (2017).
[26] E. Arca, K. Fleischer, and I. Shvets, J. Phys. Chem. C **113**, 21074 (2009).
[27] E. Arca, K. Fleischer, and I. Shvets, Thin Solid Films **555**, 9 (2014).
[28] J. Hong, K.-i. Katsumata, and N. Matsushita, Acta Mater. **103**, 844 (2016).
[29] A. T. Vai, V. L. Kuznetsov, J. R. Dilworth, and P. P. Edwards, J. Mater. Chem. C **2**, 9643 (2014).
[30] C. Park, S.-M. Lee, and W. S. Chang, Phys. Chem. Chem. Phys. **18**, 26184 (2016).
[31] F. Ruske, M. Roczen, K. Lee, M. Wimmer, S. Gall, J. Hüpkes, D. Hrunski, and B. Rech, J. Appl. Phys. **107**, 013708 (2010).
[32] D. Raoufi and T. Raoufi, Appl. Surf. Sci. **255**, 5812 (2009).
[33] M. Puchert, P. Timbrell, and R. Lamb, J. Vac. Sci. Technol. A **14**, 2220 (1996).
[34] S. Major and K. Chopra, Sol. Energy Mater. **17**, 319 (1988).
[35] M. Miki-Yoshida, F. Paraguay-Delgado, W. Estrada-Lopez, and E. Andrade, Thin Solid Films **376**, 99 (2000).
[36] A. Sarkar, S. Ghosh, S. Chaudhuri, and A. Pal, Thin Solid Films **204**, 255 (1991).

[37] L. Lutterotti, Nucl. Instrum. Methods Phys. Res., Sect. B **268**, 334 (2010).

[38] K. Ellmer, J. Phys. D: Appl. Phys. **34**, 3097 (2001).

[39] K. Ellmer and R. Mientus, Thin Solid Films **516**, 4620 (2008).

[40] Y.-J. Kim and H.-J. Kim, Mater. Lett. **41**, 159 (1999).

[41] Y. Sato, T. Yamamoto, and Y. Ikuhara, J. Am. Ceram. Soc. **90**, 337 (2007).

[42] E. Hosono, S. Fujihara, and T. Kimura, J. Mater. Chem. **14**, 881 (2004).

[43] A. Kushwaha and M. Aslam, J. Phys. D **46**, 485104 (2013).

[44] F. Ahmed, N. Arshi, M. S. Anwar, R. Danish, and B. H. Koo, Curr. Appl. Phys. **13**, S64 (2013).

[45] N. Barsan and U. Weimar, J. Electroceram. **7**, 143 (2001).

[46] G. K. Mani and J. B. B. Rayappan, Sens. Actuators B **223**, 343 (2016).

[47] H. J. Kim, I. S. Bae, S. J. Cho, J. H. Boo, B. C. Lee, J. Heo, I. Chung, and B. Hong, Nanoscale Res. Lett. **7**, 1 (2012).

[48] J. Fuggle, E. Umbach, D. Menzel, K. Wandelt, and C. Brundle, Solid State Commun. **27**, 65 (1978).

[49] S. A. Studenikin, N. Golego, and M. Cocivera, J. Appl. Phys. **84**, 2287 (1998).

[50] H. B. Zeng, G. T. Duan, Y. Li, S. K. Yang, X. X. Xu, and W. P. Cai, Adv. Funct. Mater. **20**, 561 (2010).

[51] P. Zu, Z. K. Tang, G. K. L. Wong, M. Kawasaki, A. Ohtomo, H. Koinuma, and Y. Segawa, Solid State Commun. **103**, 459 (1997).

[52] P. A. Rodnyi and I. V. Khodyuk, Opt. Spectrosc. **111**, 776 (2011).

[53] C. H. Ahn, Y. Y. Kim, D. C. Kim, S. K. Mohanta, and H. K. Cho, J. Appl. Phys. **105**, 013502 (2009).

[54] C. Barret and T. Massalski, *Structure of Metals* (Pergamon, Oxford, 1980).

[55] F. Yakuphanoglu, Y. Caglar, S. Ilican, and M. Caglar, Phys. B (Amsterdam, Neth.) **394**, 86 (2007).

[56] R. P. Wang, A. W. Sleight, R. Platzer, and J. A. Gardner, J. Solid State Chem. **122**, 166 (1996).

[57] K. Fleischer, E. Arca, C. Smith, and I. V. Shvets, Appl. Phys. Lett. **101**, 121918 (2012).

[58] J. Hupkes, J. I. Owen, S. E. Pust, and E. Bunte, ChemPhysChem **13**, 66 (2012).

[59] B. D. Viezbicke, S. Patel, B. E. Davis, and D. P. Birnie, Physica Status Solidi B **252**, 1700 (2015).

[60] E. Burstein, Phys. Rev. **93**, 632 (1954).